ASCE

Modeling Regional and Local Resilience of Infrastructure Networks Following Disruptions from Natural Hazards

Dylan Sanderson, S.M.ASCE[1]; Daniel Cox, M.ASCE[2]; Andre R. Barbosa, A.M.ASCE[3]; and John Bolte[4]

Abstract: This paper presents a framework to evaluate the regional and local resilience of infrastructure networks following disruptions from natural hazards. Herein, the regional resilience of a network relates to the accessibility of a community within a larger network, whereas the local resilience concerns the ability of a network to provide its intended service within the boundaries of a community. Using this framework, a methodology is developed to demonstrate its application to a road and highway transportation network disrupted by ground shaking and inundation under a Cascadia Subduction Zone earthquake and tsunami scenario. The regional network extents encompass the entire coast of the US state of Oregon. Embedded within this regional network are 18 local networks associated with coastal communities. Regional and local connectivity indexes are defined to identify the initial damage and then track the postdisaster recovery of the transportation network, i.e., evaluate the network resilience. The study results identify the attributes that lead to a regionally or locally resilient network and highlight the importance of considering local infrastructure networks embedded within larger regional networks. It is shown that without regional considerations, the time to recover may be severely underpredicted. The methodology is further used as a decision support tool to demonstrate how mitigation options impact the transportation network's resilience. The importance of strategically considering mitigation options is emphasized as some communities see significant reductions in time to recover, whereas others see little to no improvement. **DOI: 10.1061/(ASCE)IS.1943-555X.0000694.**

Author keywords: Community resilience; Natural hazards; Infrastructure networks; Multiple scales.

Introduction

Infrastructure networks, such as electric power, transportation, and communication, are essential for community function and resilience planning (OSSPAC 2013; NIST 2016); however, these networks are often evaluated without consideration given to the larger regional network within which they are embedded. That is, a network's spatial boundaries are limited to the spatial boundaries of the community it serves. Infrastructure networks do, however, span multiple spatial scales ranging from global accessibility, such as, ship and airplane traffic, to traversing communities and neighborhoods, including, local roads and walking trails. Further, depending on the type of infrastructure network, different services can be identified. For example, a transportation network may be used to connect people to food sources (Coveney and O'Dwyer 2009), health resources (Zhang et al. 2018), or postdisaster relief (Horner and Widener 2011). Hazards, both natural and anthropogenic, can cause damage to network components, which translates to larger system disruptions and ultimately limits the ability of a network to perform its intended service (Crucitti et al. 2004; Buldyrev et al. 2010).

When considering infrastructure networks under disruption from hazards, multiple spatial scales are of importance (Thacker et al. 2017; Zhang and Alipour 2020). For instance, following a network disruption, a community may be accessible at the regional scale, e.g., goods can reach community boundaries; however, if the local network is in poor condition, then these goods cannot be distributed throughout the community. Conversely, if the local network of a community is in good condition following a disaster, but the network is not accessible to the rest of the region, then goods cannot be transported to the community and so cannot be distributed throughout the local network. Thus, the extent to which a community is regionally or locally accessible is important.

The purpose of this paper is to present a generalized framework to simultaneously assess the regional and local resilience of infrastructure networks following disruptions from natural hazards. This framework is used to identify the attributes that lead to the regional and local resilience of networks, to demonstrate the necessity of considering local networks embedded within a larger, regional-scale network, and to evaluate the impact of alternative mitigation options on network resilience. The generalized framework is intended to be expandable across infrastructure network systems; however, a methodology is developed to demonstrate how the framework can be applied to a road and highway transportation network subject to the multihazard earthquake and tsunami threat posed by the Cascadia Subduction Zone (CSZ).

The remainder of this paper is organized as follows. The second section outlines the framework in a generalized manner and draws on examples in the literature showing how it can be applied across different infrastructure systems. The third section develops the methodology demonstrating how the framework can be applied to a road and highway transportation network. The fourth section presents results from the previous section and shows how the framework can be used to evaluate mitigation options. The fifth section presents a

[1]Ph.D. Student, School of Civil and Construction Engineering, Oregon State Univ., Corvallis, OR 97331 (corresponding author). ORCID: https://orcid.org/0000-0002-4443-7074. Email: sanderdy@oregonstate.edu

[2]CH2M Hill Professor in Civil Engineering, School of Civil and Construction Engineering, Oregon State Univ., Corvallis, OR 97331.

[3]Associate Professor, School of Civil and Construction Engineering, Oregon State Univ., Corvallis, OR 97331. ORCID: https://orcid.org/0000-0003-4547-531X

[4]Department Head, Biological and Ecological Engineering, Oregon State Univ., Corvallis, OR 97331.

Note. This manuscript was submitted on August 17, 2021; approved on February 14, 2022; published online on June 24, 2022. Discussion period open until November 24, 2022; separate discussions must be submitted for individual papers. This paper is part of the ***Journal of Infrastructure Systems***, © ASCE, ISSN 1076-0342.

discussion of this work and identifies its limitations. Finally, the sixth section summarizes the conclusions.

General Framework

Fig. 1 shows the general framework developed to assess the regional and local resilience of infrastructure networks and is broken down into three primary steps. The first step consists in organizing and collecting data. Using network and hazard data, damage to the network components is then evaluated in Step 2. The damage results in changes to network component functionality, which then determine how the network will perform as a system in Step 3. Regional and local resilience metrics are defined and tracked here, from which the multiscale resilience can be evaluated.

The first step, data collection, consists in gathering resilience planning guides and policy (Step 1a), network data (Step 1b), service information (Step 1c), and hazard data (Step 1d). Resilience planning guides and policies inform the overall analysis and can aide in identifying hazards present within a geographic region, metrics that can be tracked, or services that infrastructure networks provide (SPUR 2009; OSSPAC 2013; NIST 2016; NYC Emergency Management 2019).

Identifying the network (Step 1b) consists of specifying an infrastructure network to consider and delimitating local and regional network boundaries. The latter is necessary to consider the problem under a multiscale lens. For example, transportation networks may have regional boundaries connecting state to state (Omer et al. 2013) or local boundaries concerning accessibility within cities (Dong et al. 2016, 2020). Further, different spatial boundaries impact the ownership of infrastructure components. For example, a state may be responsible for bridges along a highway, whereas cities are responsible for bridges within city boundaries.

Here, the term *service* refers to the service that an infrastructure network was originally intended to perform (Step 1c). Infrastructure networks can perform multiple services. For example, a transportation network can be used to move people from their place of residence to places that provide health assistance (Zhang et al. 2018). Similarly, the same transportation network may be used to provide accessibility from places of residence to places of work (Omer et al. 2011). As such, identifying the service of a network also consists of identifying origins and destinations that relate to this service. The service origin and destination are dependent on the network and vice versa.

Gathering hazard data (Step 1d) consists of defining an event that prevents the network from performing its intended service (Ouyang 2014; Faturechi and Miller-Hooks 2015; Sun et al. 2018). Hazards can be either natural, such as earthquakes (Chang and Nolima 2001; Shiraki et al. 2007; Guo et al. 2017; Ishibashi et al. 2021) and hurricanes (Horner and Widener 2011; Zou and Chen 2020), or anthropogenic, such as intentional attacks (Wu et al. 2007). In the context of natural phenomena, they can often consist of multiple hazards that, if applicable, add an extra dimension to the problem (Kappes et al. 2012).

Step 2 of the framework, network component modeling and analysis, is the result of the hazard impacting the network. In the context of natural hazards, the hazard and network components are often combined via the use of fragility models (FEMA 2013; Cavalieri et al. 2014; Kakderi and Argyroudis 2014; FEMA 2015; Gidaris et al. 2017). The use of fragility models results in a probability that network components will be in or exceed a damage state (Step 2a). The damage states subsequently inform changes to the network component functionality and performance (Step 2b). The component functionality influences the component performance. In the case of transportation networks, performance may correspond to an increase in travel time along roads and bridges (Shiraki et al. 2007), whereas in power networks it may correspond to component failure (Ouyang and Dueñas-Osorio 2014; Johnson et al. 2020).

The entire network is then treated as a system in Step 3. The performance of a network as a system depends upon both individual component performance and network topology (Zhang et al. 2015). This system performance can be further evaluated at multiple scales, hence both the regional and local network performance Steps 3a and 3b. The arrow between these steps identifies interdependencies

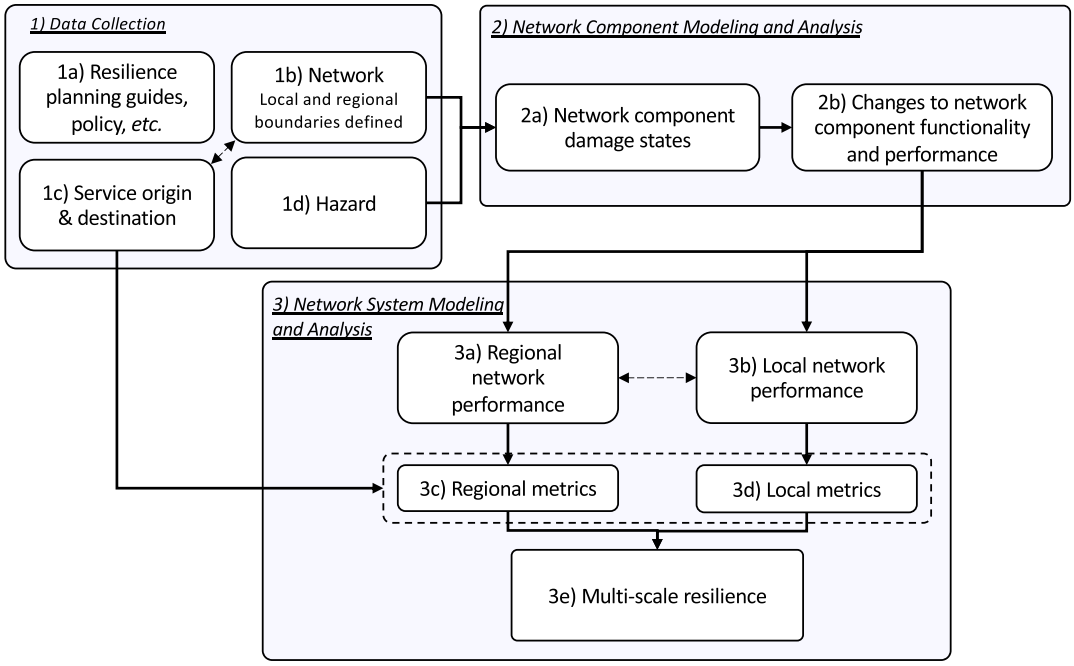

Fig. 1. Framework for assessing regional and local resilience of infrastructure networks.

between the two. Based on the network and service that are being considered, there may be either a one-way dependence, such as, the local network depends on the regional network, or a two-way dependence, such as, the local and regional networks depend upon each other. Regional and local metrics are identified (Steps 3c and 3d) to evaluate the performance of the network at multiple scales. The service origin and destination aid in identifying the local and regional metrics (Logan and Guikema 2020). Finally, the regional and local metrics are used to inform the multiscale resilience of the network (Step 3e).

Methods Applied to a Transportation Network

A methodology was developed to demonstrate how the generalized framework can be applied to a road and highway transportation network under disruption from earthquake and tsunami hazards. This section follows Steps 1 and 2 of the framework (Fig. 1).

Hazard, Network, and Service Identification

The North American Pacific Northwest is subject to the rupture of the CSZ, which can result in both strong earthquake ground shaking and tsunami inundation. The last full rupture of the CSZ occurred in 1700 and is estimated to have had a moment magnitude between 8.7 and 9.2. Further, some studies have estimated a 7% to 11% probability that a full-margin rupture will occur between 2010 and 2060 (Goldfinger et al. 2012). Local studies carried out to characterize the hazard associated with the CSZ have resulted in probabilistic hazard maps (Gonzàlez et al. 2009; Park et al. 2017), whereas at the regional scale, the hazard has been characterized based on moment magnitude. In this work, scenario-based hazard maps associated with the M9.0 earthquake and corresponding large, or L, tsunami were used (Madin et al. 2013; Priest et al. 2013) because this formed the basis of the Oregon Resilience Plan (OSSPAC 2013). In the future, a probabilistic rather than a scenario-based approach could be considered, as suggested by one of the reviewers. While a probabilistic seismic and tsunami hazard analysis (PSTHA) exists for a single community at Seaside, Oregon (Park et al. 2017) and has been used for several risk-based damage studies (e.g., Park et al. 2019; Sanderson et al. 2021), there currently exists no PSTHA for the entire Pacific Northwest.

The regional highway transportation network considered is shown in Fig. 2 and stretches from the California to Washington state borders in the north–south direction and from the Pacific coast

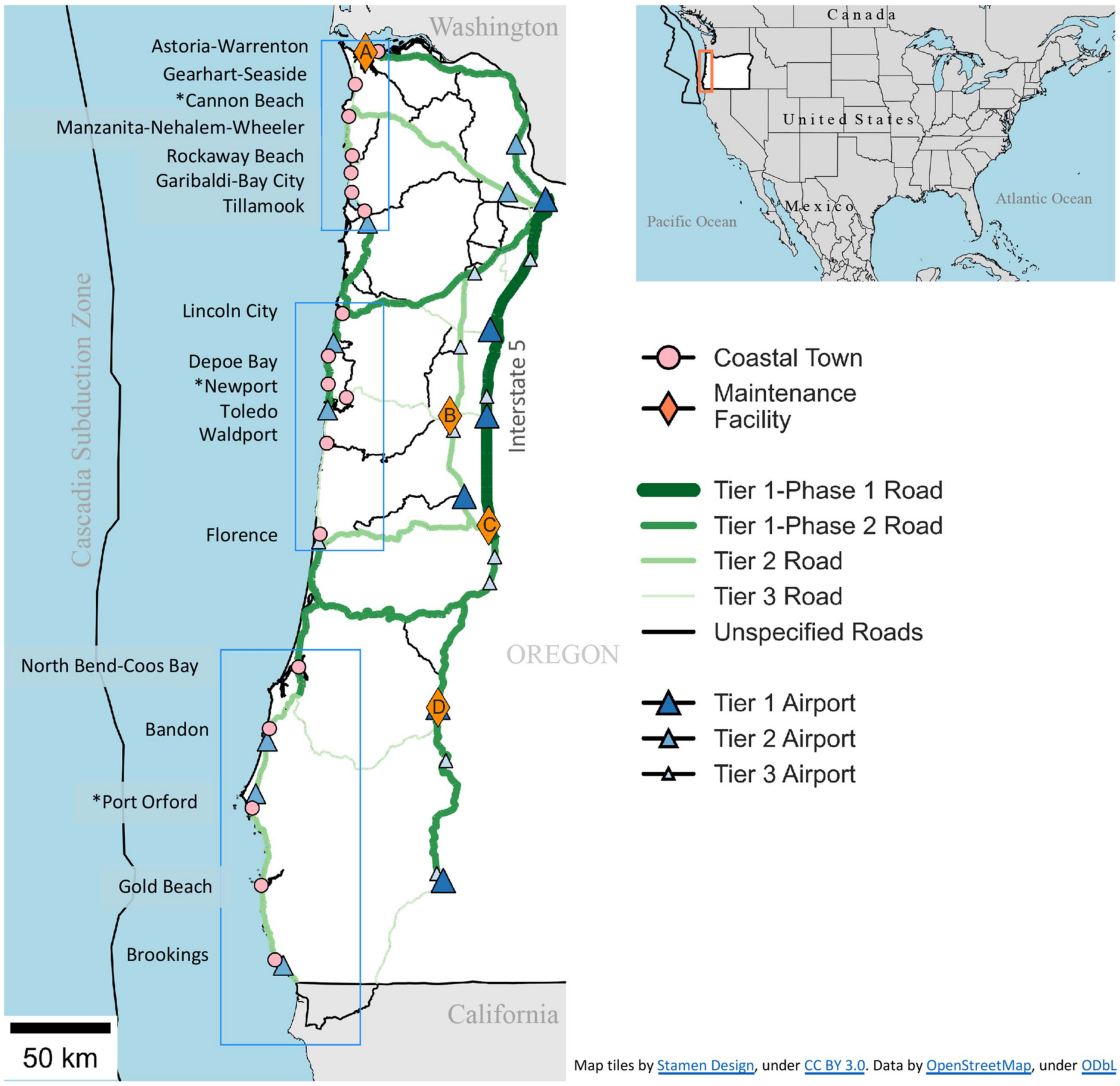

Fig. 2. Regional highway transportation network showing location of coastal communities, maintenance facilities, airports, and highway tiers. [Map tiles by Stamen Design, under CC BY 3.0 (https://creativecommons.org/licenses/by/3.0/). Data by OpenStreetMap, under ODbL.]

J. Infrastruct. Syst., 2022, 28(3): 04022021

to Interstate 5 in the east–west direction. The entire transportation network consists of 2,644 km of roads. Highways were prioritized according to a tiered approach, with Tier 1 being a backbone that allows access to most major population centers and Tier 3 providing access to all coastal communities (OSSPAC 2013). The tiered structure of the transportation network is shown in Fig. 2 and was used in this work when prioritizing restoration of highway components.

It was assumed that the role of the transportation network was to provide postdisaster aid to communities, and the location of airports were used as a proxy for supply sources. Thus, in relation to the framework in Fig. 1, airports were identified as the service origins, whereas coastal communities were identified as the service destinations. A total of 29 airports were considered and grouped into 3 tiers (Fig. 2). If an airport was located outside of the transportation network, the nearest node on the network is used as a representative point. It should be emphasized that other services, such as fuel, food, health, or access to large metropolitan areas, could be identified, although these are not considered in the illustrative example shown here.

Furthermore, locations of transportation maintenance facilities are shown in Fig. 2. Each coastal town is located within the jurisdiction of a single facility, and it was assumed that the reconstruction of local roads depended on the communities' access to their respective maintenance facility. The maintenance facilities are labeled *A*, *B*, *C*, and *D*.

Within the regional network, 18 coastal communities were considered and are shown as pink dots in Fig. 2 and summarized in Table 1. The 18 coastal communities were grouped into northern, central, and southern coasts. The northern coastal communities are closer to metropolitan areas, whereas the southern coast is considered more rural. Local network boundaries were delimited by the urban growth boundary of each community, and some coastal towns that are near others, such as Astoria-Warrenton and Gearhart-Seaside, were treated as one community for simplicity's sake. The communities range in population from 954 people (Port Orford) to 25,881 people (North Bend-Coos Bay) (US Census Bureau 2019). On average, the population of all 18 communities is 6,234 people, and there are 90.5 km of roads within each community. Information in Table 1, such as population and median income, is supplied to provide a sense of the size of each community but is not used further in this study. Fig. 3 shows the local networks for three of the coastal communities: Cannon Beach, Newport, and Port Orford. The extent of tsunami inundation and the location of bridges and airports are shown.

Probabilistic Network Component Analyses

Road and Bridge Damage Analysis

Using the hazard layers and transportation network, a probabilistic damage analysis was performed for both bridges and roads. Burns et al. (2021) conducted a multihazard damage analysis for bridges on the transportation network using, among other tools, Hazus fragility curves. The Hazus fragility curves for bridges include 28 bridge classifications that, for brevity's sake, are not presented here. Burns et al. (2021) concluded that the Hazus landslide and liquefaction fragility curves tended to overestimate bridge damage. Therefore, only ground shaking from earthquake and tsunami inundation were considered here. The resulting damage state probabilities were used in this study.

Road damage analysis was conducted using Hazus roadway fragility curves (FEMA 2013, 2015). The earthquake intensity measure was permanent ground deformation, whereas inundation depth was used for the tsunami. For consistency with the bridge damage analysis of Burns et al. (2021), landslides, lateral spreading, and liquefaction were not considered for the road damage analysis.

The bridge damage state probabilities from Burns et al. (2021) were directly sampled in a Monte Carlo simulation, whereas damage to road segments were simulated based on the approach outlined in Baker (2008) and used by Kameshwar et al. (2019) and Sanderson et al. (2021) to estimate damage to the transportation network in Seaside, Oregon. That is, the probability that the damage state, *DS*, of each road segment would exceed damage state i was computed as

$$P(DS \geq ds_i|D) = P(C_i < D) \tag{1}$$

where D = demand at the road segment; and C_i = damage capacity associated with damage state ds_i. The damage capacity of each road segment was simulated as a lognormal random variable, $LN(\cdot)$, computed as

$$C_i \sim LN(\theta_i, \beta_i) \tag{2}$$

Table 1. Sociodemographic and transportation network summary for each coastal community and entire coast

Community	Population	Median annual income (USD)	Number of nodes	Number of edges	Length roads (km)	Assigned maintenance facility
Astoria-Warrenton	15,385	52,195	1,290	1,558	208.6	A
Gearhart-Seaside	8,382	51,729	710	885	103.0	A
Cannon Beach	1,491	50,846	323	392	38.1	A
Manzanita-Nehalem-Wheeler	1,105	49,922	449	555	62.3	A
Rockaway Beach	1,166	45,781	448	545	52.5	A
Garibaldi-Bay City	2,472	53,064	354	412	43.0	A
Tillamook	5,231	41,109	330	474	48.1	A
Lincoln City	8,826	39,344	950	1,179	140.3	B
Depoe Bay	1,805	57,143	195	222	22.4	B
Newport	10,559	49,039	959	1,186	135.8	B
Toledo	3,579	60,455	320	370	46.8	B
Waldport	2,055	47,971	211	250	29.1	B
Florence	8,921	42,356	905	1,119	137.3	C
North Bend-Coos Bay	25,881	50,905	1,653	2,107	240.9	D
Bandon	3,100	32,226	456	540	61.8	D
Port Orford	954	27,500	281	337	57.1	D
Gold Beach	22,418	42,625	284	321	49.2	D
Brookings	6,431	62,384	856	985	152.6	D
Full Network	112,203	—	16,370	19,111	2,643.7	—

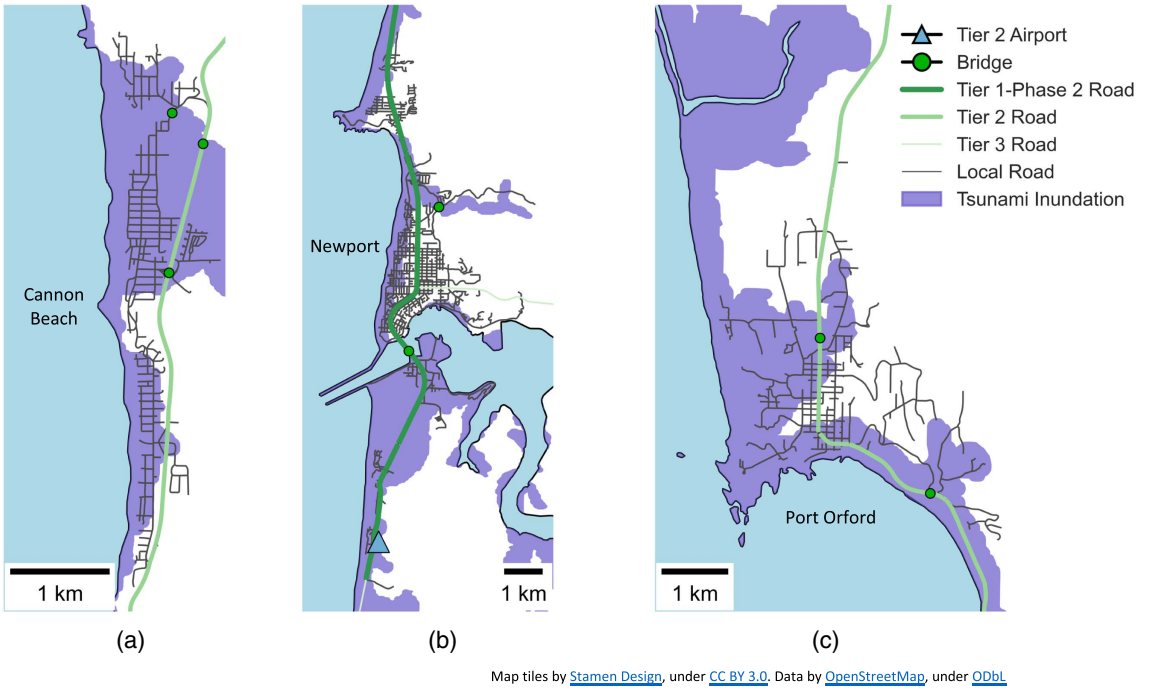

Fig. 3. Example of three local networks for (a) Cannon Beach; (b) Newport; and (c) Port Orford. [Map tiles by Stamen Design, under CC BY 3.0 (https://creativecommons.org/licenses/by/3.0/). Data by OpenStreetMap, under ODbL.]

where θ_i and β_i = median and dispersion parameters associated with damage capacity of damage state ds_i. The parameterizing medians and dispersion values are shown in Tables 2 and 3 for earthquake peak ground deformation (PGD) and tsunami inundation depth, respectively. Although correlation across road segments was not considered here, this could be accounted for by simulating a multivariate lognormal distribution (Yang et al. 2009).

A total of 1,000 iterations were performed, resulting in discrete damage states for each road and bridge and for both hazards. The multihazard damage state was then computed using the Boolean logic rules outlined in the Hazus tsunami methodology manual

$$DS_{EQ,Tsu} = \max(DS_{EQ}, DS_{Tsu}) \tag{3}$$

$$DS_{EQ,Tsu} = \text{Extensive},$$
$$\text{if: } \{DS_{EQ} = \text{moderate and } DS_{Tsu} = \text{moderate}\} \tag{4}$$

$$DS_{EQ,Tsu} = \text{Complete},$$
$$\text{if: } \{DS_{EQ} = \text{extensive and } DS_{Tsu} = \text{extensive}\} \tag{5}$$

where DS_{EQ} and DS_{Tsu} are the discrete earthquake and tsunami damage states associated with each Monte Carlo iteration. For bridges that lie on a road segment, bridge damage state is assumed rather than an underlying road damage state. If multiple bridges were located on a single road segment, the maximum damage state of the bridges was used.

Table 2. Road fragility parameterization from peak ground deformation

	Major road		Urban road	
Damage state	Median PGD (θ) (m)	Dispersion (β) (m)	Median PGD (θ) (m)	Dispersion (β) (m)
Slight	0.30	0.0178	0.15	0.0178
Moderate	0.61	0.0178	0.30	0.0178
Extensive	1.52	0.0178	0.61	0.0178
Complete	1.52	0.0178	0.61	0.0178

Restoration and Functionality

The restoration and functionality of roads and bridges were computed using Hazus restoration curves, which are represented as a normal cumulative distribution function (CDF) and parameterized via a mean and standard deviation (SD). Functionality is defined as the percentage of the component that is expected to be open or operational (FEMA 2013). Restoration curves indicate the functionality of road segments and bridges as a function of time and were computed as

Table 3. Road fragility parameterization from tsunami inundation depth (median, θ, and dispersion, β, are dependent on flow speed, u)

	Low flow ($u \le 1$ m/s)		Moderate flow ($1 < u \le 5$ m/s)		High flow ($u > 5$ m/s)	
Damage state	Median inundation depth (θ) (m)	Dispersion (β) (m)	Median inundation depth (θ) (m)	Dispersion (β) (m)	Median inundation depth (θ) (m)	Dispersion (β) (m)
Slight	0.67	0.12	0.48	0.15	0.42	0.15
Moderate	1.28	0.12	0.91	0.15	0.80	0.15
Extensive	2.07	0.12	1.48	0.15	1.30	0.15
Complete	3.35	0.12	2.39	0.15	2.10	0.15

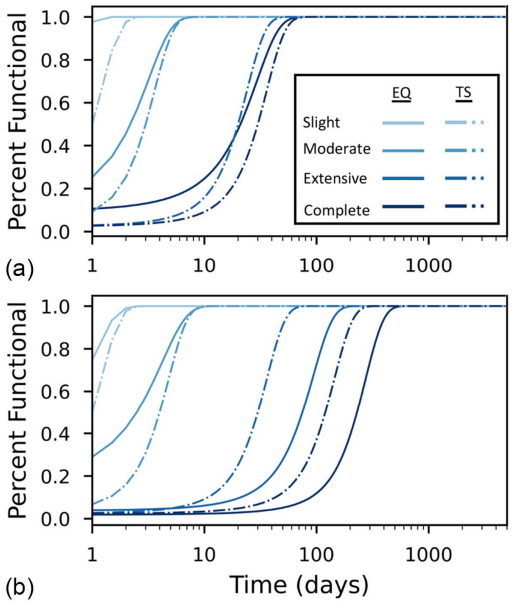

Fig. 4. Restoration curves for earthquake ground shaking (EQ) and tsunami inundation (TS) associated with (a) roads; and (b) bridges.

$$f(t) = \Phi\left(\frac{t - \mu_{ds_i}}{\sigma_{ds_i}}\right) \tag{6}$$

where $f(t)$ = functionality of the road or bridge; t = time in days after event; μ_{ds_i} and σ_{ds_i} = mean and SD associated with damage state ds_i; and $\Phi(\cdot)$ = standard normal CDF. The road and bridge restoration curves are shown in Fig. 4. The means and SDs are shown in Table 4 and vary depending on the infrastructure type (road or bridge), the type of hazard (earthquake ground motion or tsunami inundation), and the degree of damage (slight, moderate, extensive, or complete).

To account for limitations in resources, the restoration curves were modified at both the regional and local scales. At the regional scale, restoration was prioritized according to the tiers shown in Fig. 2. Each subsequent tier began restoration following all roads and bridges in the prior tier, reaching a randomly sampled functionality level. Here, the necessary functionality level to begin restoration of the following tier followed a normal distribution with a mean of 0.5 and a SD of 0.1. For example, if this value was sampled as 0.6, all Tier 1–Phase 1 roads and bridges must have reached a 0.6 functionality following the restoration curves of Fig. 4 before any Tier 1–Phase 2 road segments began restoration. The assumption is that not all roads and bridges will begin undergoing repair immediately due to limitations in resources. Note that in this work, a mean of 0.5 and SD of 0.1 were assumed; however, these values could be refined in future work based on regional preparation levels. That is, if a region has a good preparation level, then the parameterizing mean could be lower, indicating that subsequent tiers initiate their restoration process sooner. The resulting average regional functionality across all 1,000 iterations at Days 1, 60, 90, and 720 are shown in Fig. 5.

At the local scale, the functionality of roads and bridges was modified based on accessibility to maintenance facilities. It was assumed that communities rely on supplies from maintenance facilities to repair their roads and that communities located further from maintenance facilities will take longer to receive these supplies. The standard functionality was thus modified for local roads as

$$f_L(t) = f(t) \cdot \delta^k \tag{7}$$

where f was taken from Eq. (6) and δ was computed as

$$\delta(t) = \frac{T_{(o,d),0}}{T_{(o,d),t}} \tag{8}$$

where $T_{(o,d),t}$ = travel time along shortest path between origin o and destination d at time t. Here, the origin was taken as the maintenance facility and the destination as the community of interest. The reference time in the numerator is 0, indicating predisturbance travel times. As the regional network recovers, the postdisturbance travel time in the denominator approaches the predisturbance travel time and δ approaches 1. Thus, values of δ range between 0 and 1. The constant k in Eq. (7) was defined as

$$k = \begin{cases} 0.5; & T_{(o,d),0} < 1 \text{ h} \\ 1; & 1 \text{ h} \le T_{(o,d),0} < 2 \text{ h} \\ 2; & T_{(o,d),0} \ge 2 \text{ h} \end{cases} \tag{9}$$

With this formulation, the assumption behind k is that more trips can be made between communities closer to their maintenance facility than those located further away. The values of k were assumed; however, these could be refined in future work based on models that are dependent on resources available at the origin and destination. For example, if resources for repair are limited and prioritized by community, k can be a time-dependent function that approaches 0 as resources are allocated from maintenance facilities to each community. Thus, when $k = 0$, $\delta = 1$, and the local functionality is taken directly from Eq. (6). The term δ^k introduces a one-way dependence of the local network restoration on the regional network restoration. The average local functionality at Newport across all 1,000 iterations at Days 1, 60, 90, and 720 are shown in Fig. 6.

Functionality-Based Travel Time Surface

The local and regional functionality of roads and bridges were then related to increased travel times along these segments. A commonly used relationship between travel times, traffic capacities, and traffic volumes is the Bureau of Public Roads (BPR) curve (Martin and McGuckin 1998), computed as

Table 4. Road and bridge restoration curve parameterization

	Road				Bridge			
Damage state	Earthquake mean (days)	Earthquake SD (days)	Tsunami mean (days)	Tsunami SD (days)	Earthquake mean (days)	Earthquake SD (days)	Tsunami mean (days)	Tsunami SD (days)
Slight	0.9	0.05	1	0.05	0.6	0.6	1	0.5
Moderate	2.2	1.8	3	1.5	2.5	2.7	4	2
Extensive	21	16	20	10	75	42	30	15
Complete	21	15	30	15	230	110	120	60

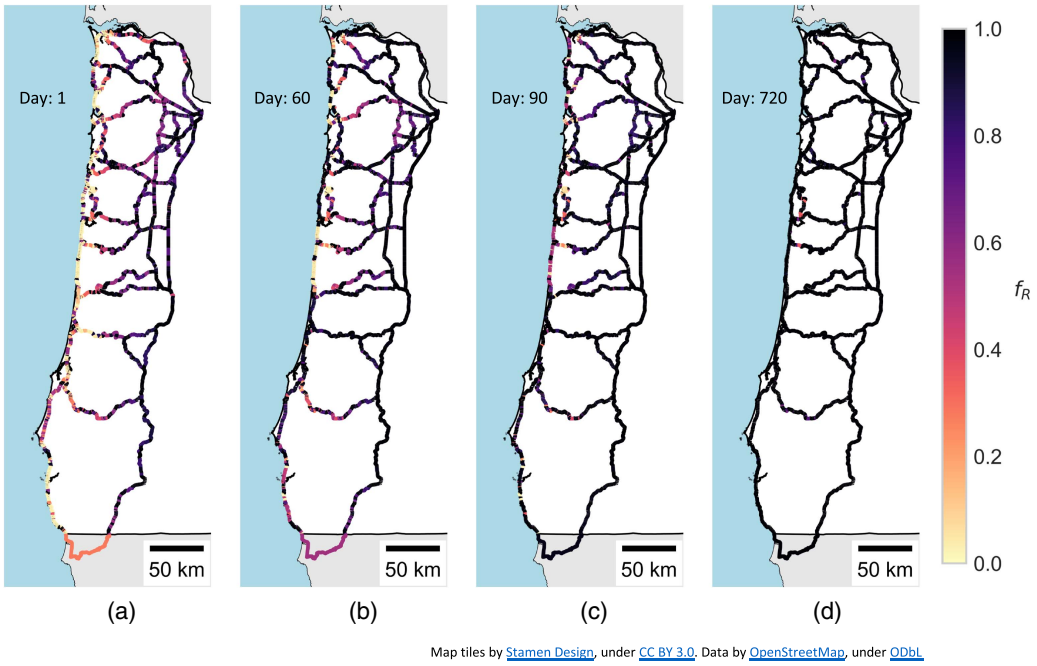

Fig. 5. Restoration of regional road network. Average functionality, fR, of regional roads and bridges is shown at (a) Day 1; (b) Day 60; (c) Day 90; and (d) Day 720. fR = 0 is nonfunctional, fR = 1 is fully functional. [Map tiles by Stamen Design, under CC BY 3.0 (https://creativecommons.org/licenses/by/3.0/). Data by OpenStreetMap, under ODbL.]

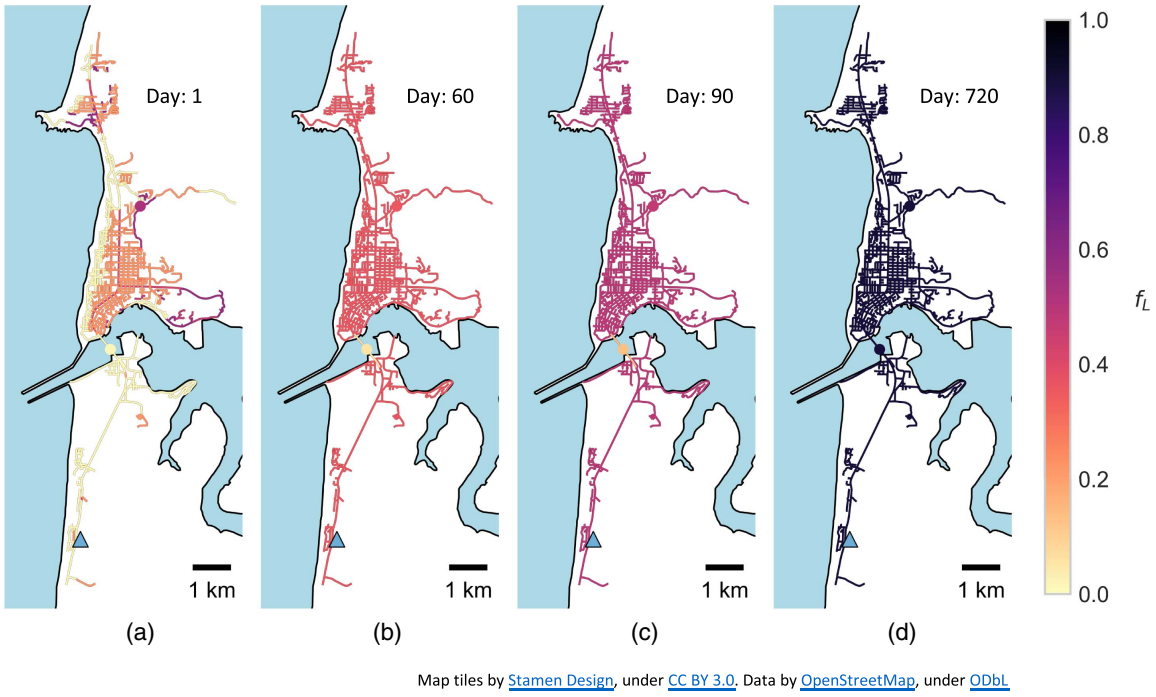

Fig. 6. Restoration of local road network for Newport. Average functionality of local roads and bridges at (a) Day 1; (b) Day 60; (c) Day 90; and (d) Day 720. fL = 0 is nonfunctional, fL = 1 is fully functional. [Map tiles by Stamen Design, under CC BY 3.0 (https://creativecommons.org/licenses/by/3.0/). Data by OpenStreetMap, under ODbL.]

$$T'_{c,s} = T'_{o,s}\left(1 + \alpha\left(\frac{v_s}{c_s}\right)^{\beta}\right) \tag{10}$$

where $T'_{c,s}$ and $T'_{o,s}$ = current and original travel times along segment s; α and β = constants typically taken to be 0.15 and 4, respectively, under normal flow conditions; and v_s and c_s = traffic volume and capacity, respectively, along segment s.

It was assumed that immediately after the rupture of the CSZ, the traffic volume on the regional road network would initially be limited and gradually return to predisturbance conditions. The traffic

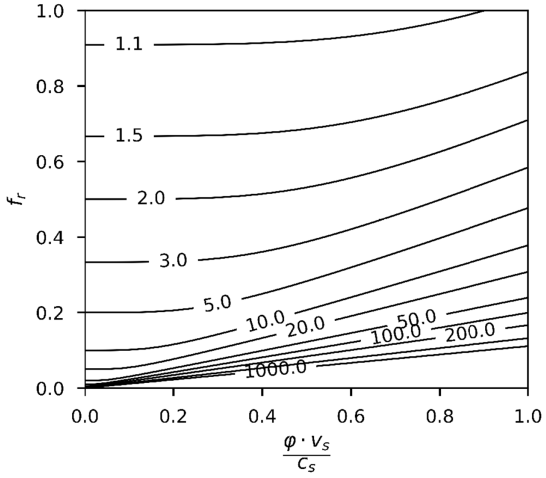

Fig. 7. Travel time surface used to relate traffic volume, traffic capacity, and functionality of roads and bridges. Each contour corresponds to values of $T'_{c,s}/T'_{o,s}$.

volume, v_s, was modified by a traffic volume multiplier, $\varphi(t)$, defined as a normal CDF with a mean of 30 days and a SD of 14 days. The traffic volume multiplier is similar to the restoration curves of Fig. 4 in that a normal CDF is used to define a unitless curve that is a function of time following the disaster. The traffic volume multiplier is simply used to reduce the traffic volume along road segment s. The parameterizing mean and SD were assumed for this work and can be refined in future work based on output from postdisaster traffic forecasting models. The BPR curve in Eq. (10) was thus modified to account for reductions in traffic volume and regional road and bridge functionality, f_R, as

$$T'_{c,s} = T'_{o,s}\left(\frac{1}{f_R} + \alpha\left(\frac{\varphi \cdot v_s}{f_R \cdot c_s}\right)^{\beta}\right) \tag{11}$$

A normalized version of Eq. (11) is shown in Fig. 7 as a function of $(\varphi \cdot v_s)/c_s$ and f_R. Each contour corresponds to values of $T'_{c,s}/T'_{o,s}$. Along the top axis, where $f_R = 1$, the standard BPR curve of Eq. (10) is obtained. Along the leftmost axis where $v \cdot \varphi = 0$, i.e., there is no traffic volume, the travel time is increased by $T'_{o,s}/f_R$. For example, a road or bridge that is 50% functional results in double the travel time. This formulation accounts for a reduction in both traffic volume and road and bridge capacity. Alternative formulations to compute postdisaster traffic volumes and travel times exist, such as gravity models and user-equilibrium traffic assignment (Shiraki et al. 2007; Guo et al. 2017); however, these were not implemented here because they require origin–destination trip assignments. The travel time surface was employed where traffic volume data were available, i.e., on the regional network. On the local networks, the travel time along a road segment was increased by $T'_{c,s} = T'_{o,s}/f_L$.

Results of Application to Transportation Network

Whereas the previous section followed Steps 1 and 2 of the generalized framework shown in Fig. 1, this section follows Step 3. That is, the network is considered as a system, and both regional and local metrics are defined to evaluate the resilience of the transportation network at multiple spatial scales. Further, it is demonstrated how this framework can be used as a decision support tool.

Regional Connectivity Index

The assumed role of the transportation network was to provide postdisaster aid to communities, and the locations of airports were used as a proxy for supply sources. Airports take on the role of service origin and were grouped into three tiers (Fig. 2). To define accessibility from these supply sources to the coastal communities, or service destinations, a regional connectivity index, RCI, was created. The RCI is based on the concept of travel time resilience (Omer et al. 2011), and was defined as

$$RCI(t) = \sum_{j \epsilon \text{Tiers}} w_j \frac{\min_{o \epsilon \text{Tier} j} T_{(o,d),0}}{\min_{o \epsilon \text{Tier} j} T_{(o,d),t}} \tag{12}$$

where $T_{(o,d),t}$ = travel time along shortest path between origin o and destination d at time t. At each time step t, the transportation network was updated according to the methodology outlined in the previous section and the shortest path recomputed using this updated network. The python package NetworkX was used to compute the shortest path between nodes (Hagberg et al. 2008). Airports were taken as the origins, whereas the communities were taken as the destinations. The time in the numerator is $t = 0$, indicating predisturbance travel times. Each airport tier was represented by the variable j, for example, $j = 1$, 2, and 3. The variable w_j is a weight that represents the importance of airport tiers, and the summation of weights across all tiers is equal to one. The weights were included to prioritize airport tiers depending on interests and features such as runway capacity and local logistics. By formulating the RCI as such, each community's index was normalized by their respective travel time under normal circumstances, for example, predisturbance travel times. This metric thus helps identify which communities were furthest displaced from their predisturbance conditions. By tracking the RCI across time and considering the network recovery, each trajectory will reapproach 1, where the postdisturbance travel times are identical to the predisturbance travel times.

Fig. 8 shows the RCI for Cannon Beach, Newport, and Port Orford for all 1,000 iterations and with equal weights across all three airport tiers. These three communities are on the northern, central, and southern coasts, respectively. The solid thick line indicates the average of all iterations at each time step, whereas the shaded region shows ± 1 SD. Fig. 8(c) shows that, on average, the RCI of Port Orford begins at approximately 0.18, indicating that across all airport tiers it takes about five times as long as the predisturbance travel time to access the community. The recovery trajectory shows that, on average, the accessibility to Port Orford is fully reestablished around 2.4 years after the CSZ. Conversely, the RCI of Cannon Beach begins on average at approximately 0.5, indicating that across all tiers the travel time to these airports is approximately doubled. Fig. 8 shows that on average Cannon Beach recovers approximately 1.75 years after the event. The low initial RCI and slower recovery time of Port Orford is due to its location within the larger regional network. The nearest Tier 1 and 3 airports are both located along Interstate 5 with no direct route to Port Orford, so the shortest path is from either the south through California or north through Bandon.

Perhaps counterintuitively, Fig. 8 shows that some of the RCI trajectories see a slight reduction before monotonically recovering. This occurs during all iterations for Newport and a handful of iterations for Cannon Beach. This is due to the form of the travel time surface and tradeoffs between road restoration and increased traffic volumes as a function of time. Port Orford does not see these reductions in RCI because it is located along the southern coast, and the southern highways are prioritized later for restoration, for example, after the traffic volumes are restored to predisturbance conditions.

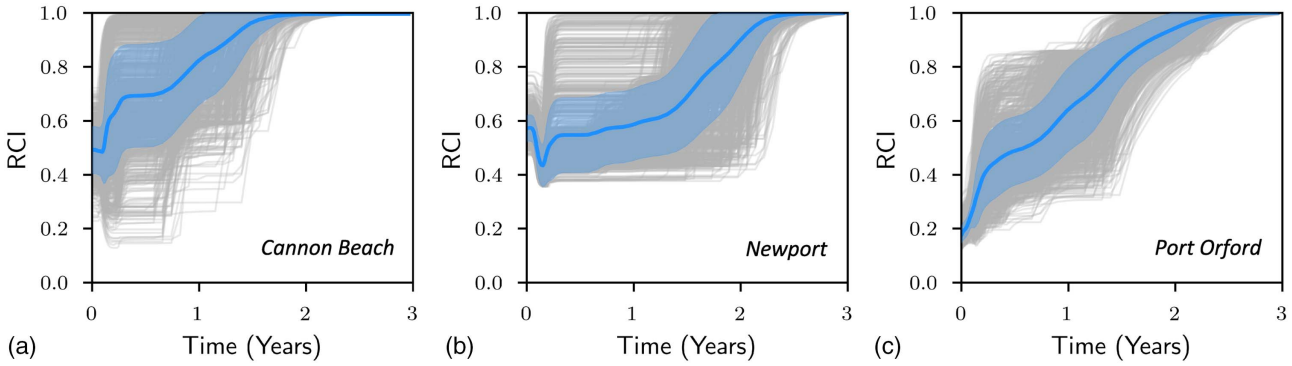

Fig. 8. Regional Connectivity Index (RCI) for (a) Cannon Beach; (b) Newport; and (c) Port Orford. Thin lines lines correspond to each iteration of the Monte Carlo simulation, the thick line is the average curve, and the shaded region indicates the ±1 SD range.

Uncertainty in the RCI trajectories of Fig. 8 stem from both uncertainty in the initial road/bridge damage states and the tiered restoration process of the regional network. Further, correlations across road segment damage states were not considered here, which contributes to the overall uncertainty when considering the network as a whole.

Local Connectivity Index

At the local scale, a local connectivity index (LCI) was introduced to measure the overall local network resilience. Similarly, based on the concept of travel time resilience, the LCI was defined as

$$LCI(t) = \left(\sum_{o\in S}\sum_{d\in S} T_{(o,d),0}\right) \Big/ \left(\sum_{o\in S}\sum_{d\in S} T_{(o,d),t}\right) \qquad (13)$$

where $T_{(o,d),t}$ = travel time along shortest path between origin o and destination d at time t. Nodes o and d are taken from a subsample of nodes, S, of the entire local network. The nodes that make up S were randomly sampled during each iteration from the local network. A reduction factor was introduced that scales down the number of nodes within each local network, here taken as 32. Thus, for example, if a local network had 1,280 nodes, a reduction factor of 32 resulted in the subsample's being composed of 40 nodes. The shortest path between all possible combinations of these 40 nodes was computed. This reduced the number of origin–destination pairs from 818,560 to 780. Sensitivity testing, although not shown here, indicated that across all iterations the use of a reduction factor of 32 provided an accurate estimate of the mean LCI while significantly reducing computational costs. Use of the reduction factor did, however, result in increased uncertainty.

The results of this LCI formulation for Cannon Beach, Newport, and Port Orford are shown in Fig. 9. The dashed-dotted line indicates the mean LCI if damage to the regional network is not considered. For these three communities, the LCI starts near 0 and recovers at different rates. The low initial LCI is driven by the network damage sustained by coastal communities as these are closer to the CSZ and hazard intensity measures are larger. The results for Newport show reductions in LCI similar to that in the RCI from Fig. 8. This is due to the one-way dependence of the local network on the regional network and accessibility to maintenance facilities. Similarly, Port Orford has a slow time to recover due to the one-way dependence.

As in Fig. 8, uncertainty in the LCI trajectories of Fig. 9 are due to the initial road/bridge damage states, no correlation across damage states, and the tiered restoration process of the regional network. Another source of uncertainty in the LCI is that a subsample of origin–destination nodes is used, rather than the entire network.

Considering Both Regional and Local Resilience

Having established both the RCI and LCI, the status of the network at multiple scales was evaluated. Fig. 10 shows the mean LCI and RCI at each time step plotted against each other for 6 of the 18 communities. The results for the mean LCI and RCI for the three communities discussed in detail previously, Cannon Beach,

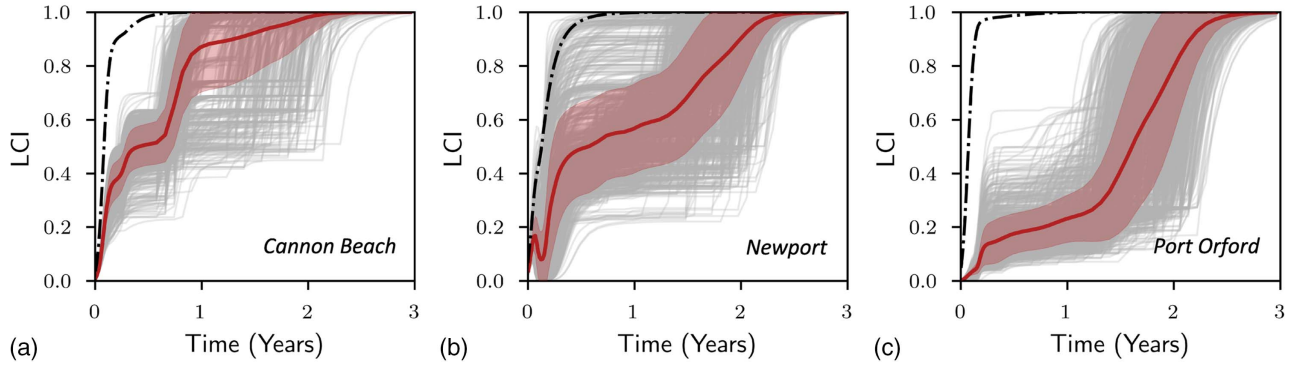

Fig. 9. Local Connectivity Index (LCI) for (a) Cannon Beach; (b) Newport; and (c) Port Orford. Thin lines correspond to each iteration of Monte Carlo simulation, the thick line is the average, and the shaded region indicates the ±1 SD range. The dashed-dotted line indicates the mean LCI when the regional network is not considered.

Newport, Port Orford, are shown in Figs. 10(a–c). Three more communities, Rockaway Beach, Lincoln City, and Toledo, are shown in Figs. 10(d–f) to demonstrate differences in recovery trajectories. Both the RCI and LCI range between 0 and 1. Each marker corresponds to Days 1, 30, 60, 180, 360, and 720. Four quadrants are identified in Fig. 10. A trajectory that passes through the lower right quadrant indicates that the local recovery outpaces the regional recovery, and thus a community may have reestablished its local network but remain isolated from the rest of the region. Conversely, a trajectory that passes through the upper left quadrant conveys the opposite. That is, the community is accessible from the rest of the region, but the local network has not been reestablished to the same level of functionality.

Of the communities shown in Fig. 10, Port Orford in Fig. 10(c) has a regional recovery that initially outpaces the local recovery, thereby indicating that aid from the airports may be able to reach the community, but the local network has still not been repaired to the same level of functionality. Conversely, Toledo, shown in Fig. 10(f), exhibits the opposite trend. That is, the local recovery outpaces the regional recovery, indicating that the local network is recovering quicker; however, the community has poor access to airports throughout the region.

Both Cannon Beach in Fig. 10(a) and Newport in Fig. 10(b) show a robust initial RCI compared to the LCI. For both communities, the regional recovery is initially slow while the local network is being repaired. The dips in the RCI and LCI that were previously identified for Newport are shown in Newport's trajectory, as both the RCI and LCI decrease around day 30 before beginning a monotonic recovery.

Rockaway Beach, Fig. 10(d), and Lincoln City, Fig. 10(e), show recovery trajectories that are both near to a 45° line, indicating that the regional and local connectivity indexes are on pace with each other. While these trajectories appear nearly identical, the temporal component of these plots should be considered. Whereas Lincoln City is approaching a full recovery around Day 180, Rockway Beach is only halfway recovered.

The recovery trajectories of the six communities shown in Fig. 10 emphasize how communities recover not in isolation from the rest of the region, but in concert with the regional network. Aside from Toledo [Fig. 10(f)], the local recovery of the communities shown in Fig. 10 is highly dependent on the recovery of the regional network. That is, the regional recovery either outpaces or is in line with the local recovery. This further emphasizes the need for local networks to be considered in a larger network following regional disasters.

The RCI and LCI can also be used to determine the time until a community returns to some index threshold at both the regional and local scales. Fig. 11 shows, for all 18 communities, the time until the RCI exceeds 0.75 [Fig. 11(a)], the LCI exceeds 0.75 [Fig. 11(b)], and both the RCI and LCI exceed 0.75 [Fig. 11(c)]. The selection of the value of 0.75 is subjective and was selected because it corresponds to travel times that are 1.33 times longer than predisturbance conditions and are thus approaching *near-normal*. While not shown here, a sensitivity analysis indicates that regardless of whether 0.7, 0.75, 0.8, or 0.9 is chosen as an exceedance threshold for the LCI/RCI, the relative comparisons across communities remain similar. The figure is oriented such that each community is shown from north (Astoria-Warrenton) to south (Brookings). Uncertainty is quantified via violin plots, which are nonparametric distributions of all 1,000 iterations. The mean time until exceedance is shown via the markers.

Considering the time until the RCI exceeds 0.75 in Fig. 11(a), notable trends between the location of a community within the regional network and the time to recover can be obtained. The faster recovering communities are either (1) located along a Tier 1–Phase 2 road, including, Astoria-Warrenton, Tillamook, Lincoln City,

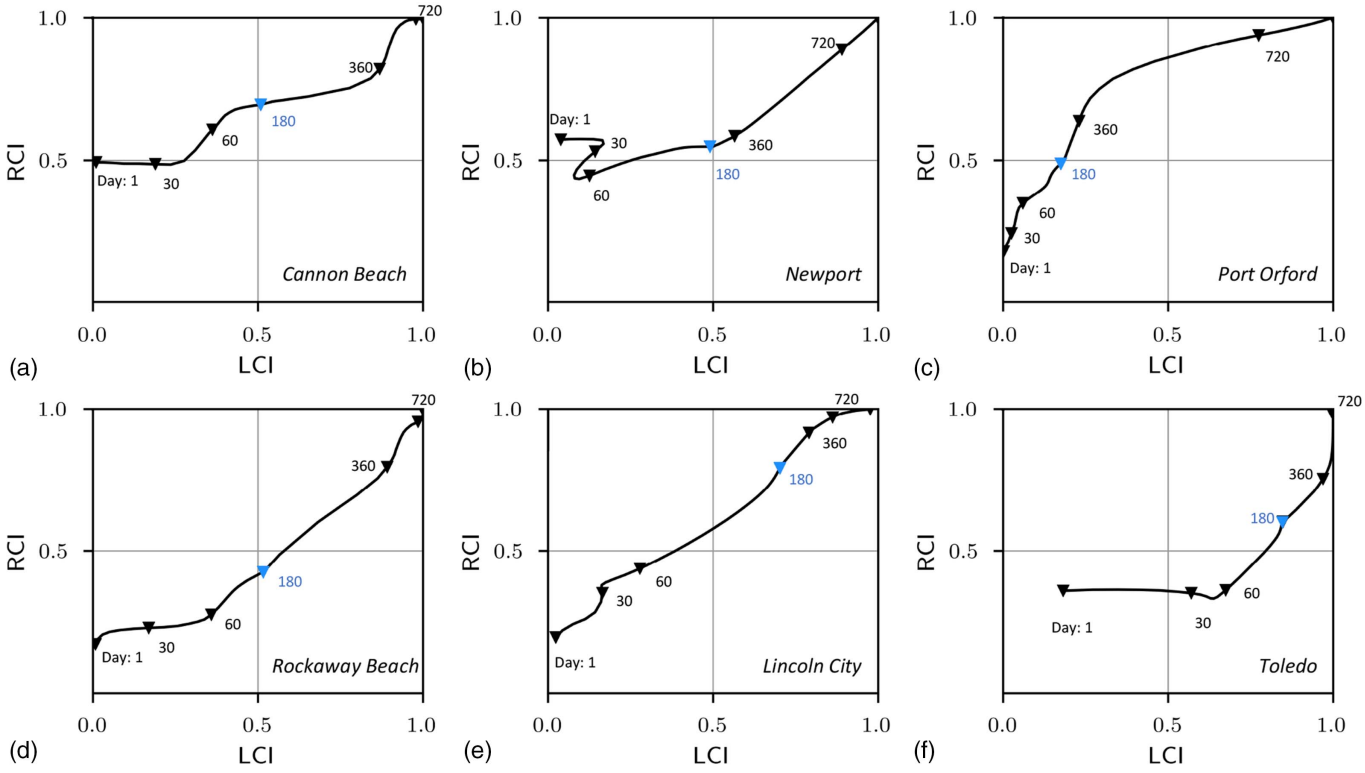

Fig. 10. RCI versus LCI recovery trajectories for (a) Cannon Beach; (b) Newport; (c) Port Orford; (d) Rockaway Beach; (e) Lincoln City; and (f) Toledo.

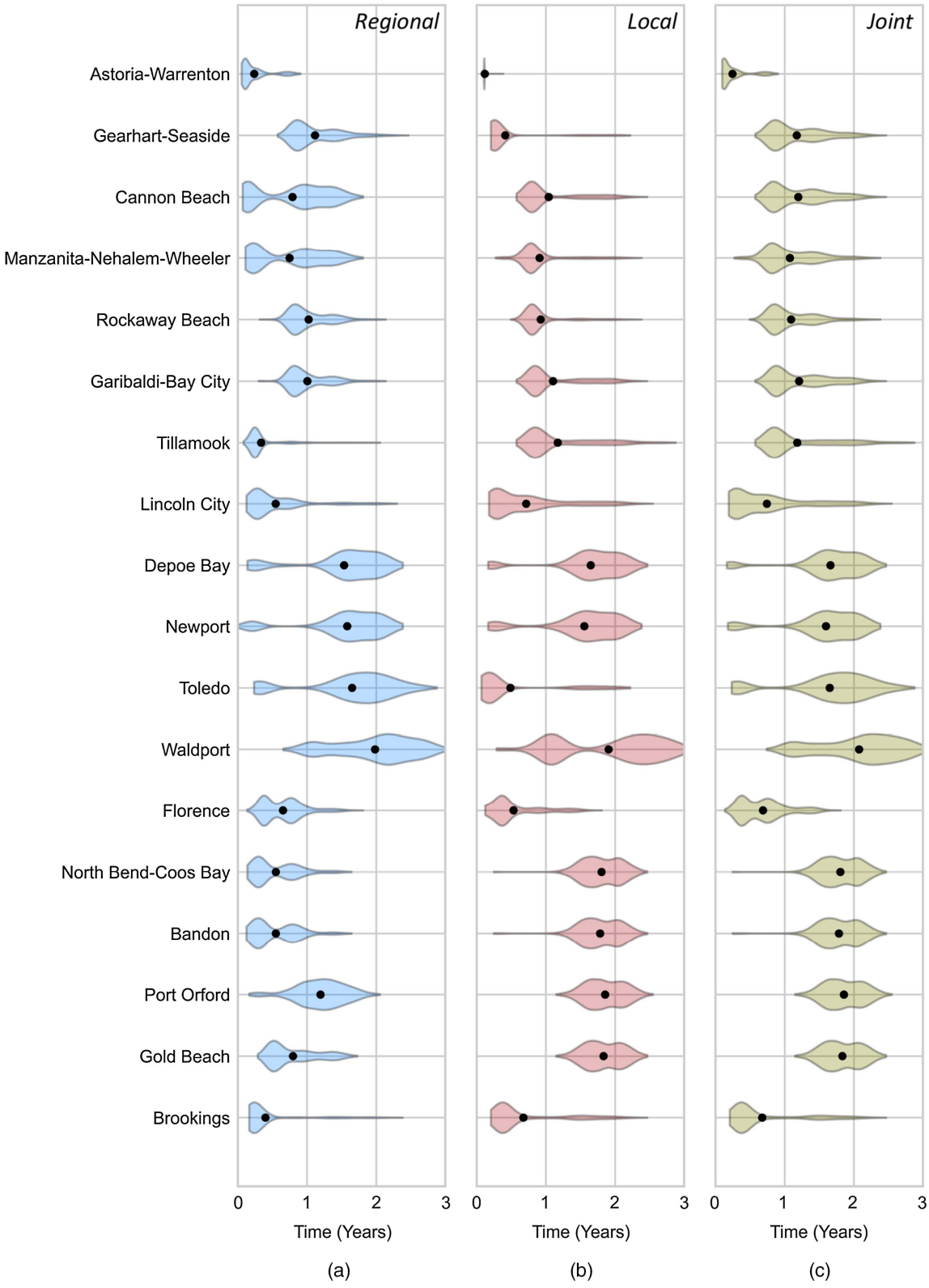

Fig. 11. Time in years required for connectivity index to exceed 0.75 for (a) RCI; (b) LCI; and (c) joint RCI and LCI. Dots indicate mean time to exceed 0.75.

Florence, and North Bend-Coos Bay, or (2) one where the connecting roads to the rest of the region are not located along the coast, including, Bandon and Brookings. A handful of these communities share both features. For example, Astoria-Warrenton is located at the tail of a Tier 1–Phase 2 road that does not run directly along the coast and, subsequently, results in the fastest regional recovery. It is interesting to note that, although a community may be located on a Tier 1–Phase 2 road, this does not necessarily guarantee a fast

recovery, for example, Newport. This is due to the fact that the connecting roads are located along the coast and thus subject to larger hazard intensity measures.

Fig. 11(c) shows that Astoria-Warrenton has the quickest average joint time to recover, followed by Florence, Brookings, and Lincoln City. The fast recovery of Astoria-Warrenton is driven by regional recovery and at the local scale by the maintenance facility located within the urban growth boundary. Because there is a maintenance facility located within the urban growth boundary, the local restoration follows the Hazus restoration curves exactly.

Like Astoria-Warrenton, Florence is located at the tail of a Tier 1–Phase 2 road and exhibits a fast recovery. Compared to the neighboring communities, Waldport and North Bend-Coos Bay, the recovery of Florence is significantly faster. This is driven by a couple of factors. On one hand, Waldport is only accessible via Tier 3 and undefined roads, so the regional recovery is slow. This is apparent in Fig. 11(a), as the mean regional time to recover for Waldport is approximately 2 years compared to less than a year for Florence. South of Florence, North Bend-Coos Bay is also situated on a Tier 1–Phase 2 road and can be seen to have a similar regional recovery time. However, the local recovery of North Bend-Coos Bay is nearly a year longer than that of Florence. This variation in local recovery between the two communities is due to the fact that Florence and North Bend-Coos Bay are in different maintenance facility districts (Table 1; Fig. 2). In this case, Florence has better accessibility to the assigned maintenance facility *C*, compared to that of North Bend-Coos Bay which is assigned maintenance facility *D*.

The community of Brookings has a short average recovery time because the Tier 2 airport located within the urban growth boundaries, and the community is not subject to liquefaction. Because of the latter, only the tsunami hazard impacts the performance of the local road network.

Each of the coastal communities can be delimited as northern coast (Astoria-Warrenton to Tillamook), central coast (Lincoln City to Florence), and southern coast (North Bend-Coos Bay to Brookings). Considering these groupings, trends in time to recover can be identified. For example, amongst the northern coastal communities, Gearhart-Seaside to Tillamook have similar recovery times, whereas Astoria-Warrenton recovers nearly a year before. For the central coastal communities, both Lincoln City and Florence recover faster than the other four communities. And for the southern coast, Brookings recovers faster. The fast recovery time of these four communities within their respective northern, central, and southern coastal distinctions may indicate that these communities could be used as coastal hubs for postdisaster restoration efforts.

Decision Support

Two variations in how this framework can be used as a decision support tool are shown in Fig. 12. Fig. 12(a) shows how the weighting parameter of Eq. (12) impacts the mean time to restore the RCI to 0.75. The points corresponding to *All Tiers* are the same as the mean values from Fig. 11(a), in which all airport tiers were weighted equally. The points labeled *Any Tier* correspond to the minimum time for the RCI to exceed 0.75 considering each airport tier individually. Interestingly, northern coastal communities see little to no variation when considering each airport tier individually. Conversely, the central and southern coastal communities do see deviations, indicating that they may be accessible to certain airports, but not to all. Tier 2 and 3 airports are located along the coast in some central and southern coastal communities. Thus, if these airports can accommodate postdisaster needs, the southern coastal communities may recovery just as fast as, if not faster than, the northern coastal communities.

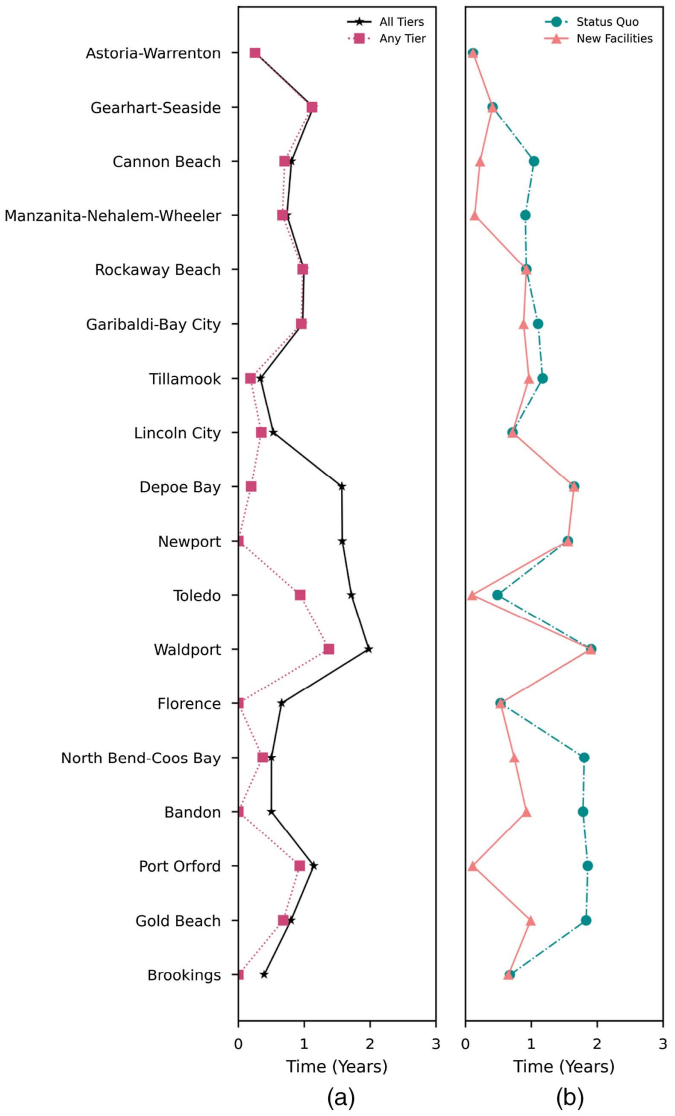

Fig. 12. Example of using framework as decision support tool: (a) time for RCI to exceed 0.75 considering different airport tier weightings; and (b) time for LCI to exceed 0.75 under both status quo conditions and with additional maintenance facilities.

Fig. 12(b) shows the effect that adding additional maintenance facilities has on the time to restore the LCI to 0.75. This further highlights dependencies between the regional and local networks in that the maintenance facilities located throughout the region have an impact on local network restoration. In addition to the four maintenance facilities shown in Fig. 2, three additional facilities were added to the network in the communities of Wheeler, Toledo, and Port Orford. Fig. 12(b) shows the mean time until the LCI exceeds 0.75 for both the status quo conditions, e.g., the same points shown in Fig. 11(b), and with the addition of three new maintenance facilities. The beneficial effect that a new maintenance facility in Port Orford has on the southern coastal communities is apparent as these communities see a reduction in the time until the LCI exceeds 0.75. Northern coastal communities, Manzanita-Nehalem-Wheeler, and Cannon Beach see improvements with the addition of a maintenance facility in Wheeler. The remaining communities do not see as much of an improvement either because they already have a short time to recover, or their assigned maintenance facility is the same as the status quo conditions.

Discussion

The methodology that was developed can be used to aid discussions in mitigation planning along multiple fronts. First, due to increases in travel time that may result from natural hazards, individuals residing in communities may face a sense of so-called islanding or isolation from the rest of the region or their local community. For example, if the travel time between two communities begins to increase beyond expectations, such as, what used to be a 1-h trip now takes 5 h, individuals may feel isolated from the rest of the region. Planning guides have alluded to this concept without explicitly defining what constitutes an *island* (CH2M Hill 2012; CREW 2013; OSSPAC 2013). The RCI and LCI could serve as the means to quantify this. For example, decision makers may determine that if a community is below a threshold of 0.2, for instance, a fivefold increase in travel time relative to predisturbance conditions, then this establishes an island. Further, rather than a connectivity index, an islanding index could be formulated, for example, one minus the RCI or LCI, to define the severity of islanding.

In addition, the results obtained from this methodology emphasize the necessity of considering postdisaster performance and restoration of local networks within a larger regional setting. The use of restoration curves without consideration given to regional-level restoration efforts may lead to underpredicting the time to recover. It was shown that by applying Hazus restoration curves without regional considerations, the LCI will approach 90% recovery within a couple of months. With regional considerations, the framework presented here estimates recovery times well beyond 1 year for most coastal communities. Future research could aim to refine the postdisaster dependencies and interdependencies of local networks within larger regional settings.

Some assumptions were made to implement the methodology. First, no damage to airports was considered, and it was assumed that temporary measures were employed to quickly resume operations. This has been observed in connection with air traffic control towers in prior earthquakes (e.g., Almufti et al. 2014). Damage to airports could, however, be considered in future work using airport fragility curves and restoration functions similar to those used for roads and bridges. Further, assumptions in the restoration process were made. To account for limitations in resources at the regional scale, the restoration curves were modified by assuming that the restoration of higher priority tiers needed to reach a randomly sampled functionality level. Alternative approaches to quantifying the restoration of infrastructure systems exist and could be used in future work (Costa et al. 2021; Wang and van de Lindt 2021). Further, the traffic volumes on the road network were assumed to be zero immediately after the event and to slowly recover to predisturbance conditions. Alternative approaches to accounting for postdisaster traffic volumes exist and could also be incorporated (Dong et al. 2016; Guo et al. 2017). Minor assumptions include both the location of maintenance facilities and the grouping of nearby communities into one large community, for example, Astoria-Warrenton and Gearhart-Seaside.

Despite these assumptions, the framework can still aid stakeholders in mitigation planning. Because the recovery of infrastructure systems following disasters involves multiple actors that do not follow physical laws, there is considerable uncertainty and complexity regarding both accurate and precise estimates of the time it takes to recover. As such, this framework is not intended to be predictive in the sense that other models of physical processes may be. Rather, the framework is intended to be used to make comparisons of local versus regional resilience of a given community, for example, community *A* is more regionally resilient than it is locally resilient, and comparisons across communities, such as, community *A* is more regionally/locally resilient than community *B*.

In addition to addressing the limitations, future work could also include considering a larger transportation network that extends both further east and into neighboring states. A multistate network may aid in a more concerted effort to reduce the impacts of large-scale events. Additionally, critical facilities such as fire stations and hospitals are used in disaster research and, while important, overlook what community members may value. Thus, this work has the potential to be expanded beyond an engineering perspective to a larger interdisciplinary perspective. Similar to how previous work considered equitable access to various services via transportation networks (Logan and Guikema 2020), interview data on what community members value could be geocoded and used within this methodology to determine how accessible these locations are for members of a community.

Conclusions

This paper presented a multiscale framework for simultaneously assessing the regional and local resilience of infrastructure networks following disruptions from natural hazards. The framework is intended to be expandable across different types of infrastructure networks. A methodology was developed from the generalized framework to demonstrate how it can be applied to a road and highway transportation network under disruption from a multihazard CSZ earthquake ground shaking and tsunami inundation scenario. With airports used as proxies for the location of supply sources, the application of this methodology provides insights into the resilience of a transportation network at multiple spatial scales. Considering the problem under a multiscale lens results in both regional and local metrics related to increases in travel times. The regional metric of a community, the RCI, considered accessibility from the community boundaries to airports, whereas the local metric, the LCI, considered accessibility within the urban growth boundary of the community itself. Comparing the two metrics together yields insights into how a community will fare immediately after an event and during the recovery process at both spatial scales.

By developing a methodology for a transportation network from the generalized framework, several conclusions can be drawn:

1. *The postdisaster performance and recovery of local networks should be considered in the context of a larger regional network*. The methodology incorporated a one-way dependence of the restoration of local networks on access to resources within a regional network. By comparing the results in this paper to previous work in which regional networks were not considered, the time to recover for a single community was shown to be four times longer than previously estimated. Further, the recovery of local networks was shown to vary across communities, indicating that communities are sensitive to where they are situated within regional networks.
2. *Attributes that lead to regional and local resilience differ*. It was shown that regionally resilient communities are not guaranteed to be locally resilient, and vice versa. Communities experiencing fast regional recovery had access to roads that were both identified as higher priority for restoration and located in areas subject to smaller hazard intensity measures. Communities that quickly recovered locally were shown to be highly dependent on access to maintenance facilities. In addition, select communities were shown to have attributes that led to a faster recovery relative to neighboring communities and could potentially serve as hubs for restoration efforts.

3. *Implementation of mitigation options should be strategically considered and do not guarantee an improvement in the time it takes to recover.* It was shown that adding additional maintenance facilities impacted some communities, but others saw little to no improvements. In this work, communities that are more rural saw improvements in time to recover when an additional maintenance facility was added in the region. Conversely, communities closer to metropolitan areas saw minimal improvement.

Data Availability Statement

All data, models, and code that support the findings of this study are available from the corresponding author upon reasonable request.

Acknowledgments

We acknowledge funding that supported this research in part from Oregon Sea Grant under Award NA18OAR170072 (CDFA 11.417) from the National Oceanic and Atmospheric Administration's National Sea Grant College Program, the US Department of Commerce, and by appropriations made by the Oregon State Legislature. We further acknowledge funding as part of Cooperative agreement 70NANB15H044 between the National Institute of Standards and Technology (NIST) and Colorado State University through a subaward to Oregon State University. The content expressed in this paper are the views of the authors and do not necessarily represent the opinions or views of NIST or the US Department of Commerce.

References

Almufti, I., A. Barbosa, J. Bray, T. Dawson, J. Marrow, M. Mieler, C. Scawthorn, and M. Yashinsky. 2014. *M 6.0 South Napa Earthquake of August 24, 2014*. Oakland, CA: Earthquake Engineering Research Institute.

Baker, J. 2008. "Introducing correlation among fragility functions for multiple components." In *Proc., 14th World Conf. on Earthquake Engineering*, 12–17. Harbin, China: Chinese Association of Earthquake Engineering.

Buldyrev, S., R. Parshani, G. Paul, E. Stanley, and S. Havlin. 2010. "Catastrophic cascade of failures in interdependent networks." *Nature* 464 (7291): 1025–1028. https://doi.org/10.1038/nature08932.

Burns, P. O., A. R. Barbosa, M. J. Olsen, and H. Wang. 2021. "Multihazard damage and loss assessment of bridges in a highway network subjected to earthquake and tsunami hazards." *Nat. Hazard. Rev.* 22 (2): 05021002. https://doi.org/10.1061/(ASCE)NH.1527-6996.0000429.

Cavalieri, F., P. Franchin, and P. Pinto. 2014. "Fragility functions of electric power stations." *SYNER-G: Typology definition and fragility functions for physical elements at seismic risk*, 157–185. New York: Springer.

CH2M Hill. 2012. *Seismic lifelines evaluation, vulnerability synthesis, and identification*. Corvallis, OR: CH2M Hill.

Chang, S., and N. Nojima. 2001. "Measuring post-disaster transportation system performance: The 1995 Kobe earthquake in comparative perspective." *Transp. Res. Part A Policy Pract.* 35 (6): 475–494. https://doi.org/10.1016/S0965-8564(00)00003-3.

Costa, R., T. Haukaas, and S. Chang. 2021. "Agent-based model for post-earthquake housing recovery." *Earthquake Spectra* 37 (1): 46–72. https://doi.org/10.1177/8755293020944175.

Coveney, J., and L. A. O'Dwyer. 2009. "Effects of mobility and location on food access." *Health Place* 15 (1): 45–55. https://doi.org/10.1016/j.healthplace.2008.01.010.

CREW (Cascadia Region Earthquake Working Group). 2013. *Cascadia Subduction Zone Earthquakes: A magnitude 9.0 earthquake scenario*. DOGAMI Open File Rep. O-13-22. Portland, OR: Dept. of Geology and Mineral Industries.

Crucitti, P., V. Latora, and M. Marchiori. 2004. "Model for cascading failures in complex networks." *Phys. Rev. E* 69 (4): 045104. https://doi.org/10.1103/PhysRevE.69.045104.

Dong, S., A. Mostafizi, H. Wang, and P. Bosa. 2016. "Post-disaster mobility in disrupted transportation network: Case study of Portland, Oregon." In *Proc., Int. Collaboration in Lifeline Earthquake Engineering 2016*, 501–507. Reston, VA: ASCE.

Dong, S., A. Mostafizi, H. Wang, J. Gao, and X. Li. 2020. "Measuring the topological robustness of transportation networks to disaster-induced failures: A percolation approach." *J. Infrastruct. Syst.* 26 (2): 04020009. https://doi.org/10.1061/(ASCE)IS.1943-555X.0000533.

Faturechi, R., and E. Miller-Hooks. 2015. "Measuring the performance of transportation infrastructure systems in disasters: A comprehensive review." *J. Infrastruct. Syst.* 21 (1): 04014025. https://doi.org/10.1061/(ASCE)IS.1943-555X.0000212.

FEMA. 2013. *Tsunami methodology technical manual*. Washington, DC: FEMA.

FEMA. 2015. *Hazus—MH 2.1 technical manual, multi-hazard loss estimation methodology, earthquake manual*. Washington, DC: FEMA.

Gidaris, I., J. Padgett, A. Barbosa, S. Chen, D. Cox, B. Webb, and A. Cerato. 2017. "Multiple-hazard fragility and restoration models of highway bridges for regional risk and resilience assessment in the United States: State-of-the-art review." *J. Struct. Eng.* 143 (3): 04016188. https://doi.org/10.1061/(ASCE)ST.1943-541X.0001672.

Goldfinger, C., et al. 2012. *Turbidite event history—Methods and implications for Holocene paleoseismicity of the Cascadia Subduction Zone*. Rep. No. 1661-F. Reston, VA: USGS.

Gonzàlez, F., et al. 2009. "Probabilistic tsunami hazard assessment at Seaside, Oregon, for near- and far-field seismic sources." *J. Geophys. Res.* 114 (C11): 1–19. https://doi.org/10.1029/2008JC005132.

Guo, A., Z. Liu, S. Li, and H. Li. 2017. "Seismic performance assessment of highway bridge networks considering post-disaster traffic demand of a transportation system in emergency conditions." *Struct. Infrastruct. Eng.* 13 (12): 1523–1537. https://doi.org/10.1080/15732479.2017.1299770.

Hagberg, A., D. Schult, and P. Swart. 2008. "Exploring network structure, dynamics, and function using NetworkX." In *Proc., 7th Python in Science Conf.*, edited by G. Varoquaux, T. Vaught, and J. Millman, 11–15. Oak Ridge, TN: USDOE.

Horner, M., and M. Widener. 2011. "The effects of transportation network failure on people's accessibility to hurricane disaster relief goods: A modeling approach and application to a Florida case study." *Nat. Hazard.* 59 (3): 1619–1634. https://doi.org/10.1007/s11069-011-9855-z.

Ishibashi, H., M. Akiyama, D. Frangopol, S. Koshimura, T. Kojima, and K. Nanami. 2021. "Framework for estimating the risk and resilience of road networks with bridges and embankments under both seismic and tsunami hazards." *Struct. Infrastruct. Eng.* 17 (4): 494–514. https://doi.org/10.1080/15732479.2020.1843503.

Johnson, B., V. Chalishazar, E. Cotilla-Sanchez, and T. Brekken. 2020. "A Monte Carlo methodology for earthquake impact analysis on the electrical grid." *Electr. Power Syst. Res.* 184 (Jul): 106332. https://doi.org/10.1016/j.epsr.2020.106332.

Kakderi, K., and S. Argyoudis. 2014. "Fragility functions of water and waste-water systems." In *SYNER-G: Typology definition and fragility functions for physical elements at seismic risk*, 221–258. Berlin: Springer. https://doi.org/10.1007/978-94-007-7872-6.

Kameshwar, S., D. Cox, A. Barbosa, K. Farokhnia, H. Park, M. Alam, and J. van de Lindt. 2019. "Probabilistic decision-support framework for community resilience: Incorporating multi-hazards, infrastructure interdependencies, and resilience goals in a Bayesian network." *Reliab. Eng. Syst. Saf.* 191 (Nov): 106568. https://doi.org/10.1016/j.ress.2019.106568.

Kappes, M., M. Keiler, K. von Elverfeldt, and T. Glade. 2012. "Challenges of analyzing multi-hazard risk: A review." *Nat. Hazard.* 64 (2): 1925–1958. https://doi.org/10.1007/s11069-012-0294-2.

Logan, T., and S. Guikema. 2020. "Reframing resilience: Equitable access to essential services." *Risk Anal.* 40 (8): 1538–1553. https://doi.org/10.1111/risa.13492.

Madin, I., W. Burns, and V. McConnell. 2013. *Ground motion, ground deformation, tsunami inundation, coseismic subsidence, and damage potential maps for the 2012 Oregon Resilience Plan for Cascadia*

Subduction Zone Earthquakes. Portland, OR: Dept. of Geology and Mineral Industries.
Martin, W., and N. McGuckin. 1998. Vol. 365 of *Travel estimation techniques for urban planning*. Washington, DC: National Academy Press.
NIST. 2016. Vol. 1 of *Community resilience planning guide for buildings and infrastructure systems*. Washington, DC: NIST.
NYC (New York City) Emergency Management. 2019. *NYC's risk landscape: A guide to hazard mitigation*. New York: NYC Emergency Management.
Omer, M., A. Mostashari, and R. Nilchiani. 2011. "Measuring the resiliency of the Manhattan points of entry in the face of severe disruption." *Am. J. Eng. Appl. Sci.* 4 (1): 153–161. https://doi.org/10.3844/ajeassp.2011.153.161.
Omer, M., A. Mostashari, and R. Nilchiani. 2013. "Assessing resilience in a regional road-based transportation network." *Int. J. Ind. Syst. Eng.* 13 (4): 389–408. https://doi.org/10.1504/IJISE.2013.052605.
OSSPAC (Oregon Seismic Safety Policy Advisory Commission). 2013. *The Oregon resilience plan: Reducing risk and improving recovery for the next Cascadia Subduction earthquake and tsunami*. Salem, OR: OSSPAC.
Ouyang, M. 2014. "Review on modeling and simulation of interdependent critical infrastructure systems." *Reliab. Eng. Syst. Saf.* 121 (Jan): 43–60. https://doi.org/10.1016/j.ress.2013.06.040.
Ouyang, M., and L. Dueñas-Osorio. 2014. "Multi-dimensional hurricane resilience assessment of electric power systems." *Struct. Saf.* 48 (May): 15–24. https://doi.org/10.1016/j.strusafe.2014.01.001.
Park, H., M. Alam, D. Cox, A. Barbosa, and J. van de Lindt. 2019. "Probabilistic seismic and tsunami damage analysis (PSTDA) of the Cascadia Subduction Zone applied to Seaside, Oregon." *Int. J. Disaster Risk Reduct.* 35 (Apr): 101076. https://doi.org/10.1016/j.ijdrr.2019.101076.
Park, H., D. Cox, M. Alam, and A. Barbosa. 2017. "Probabilistic seismic and tsunami hazard analysis conditioned on a Megathrust rupture of the Cascadia subduction zone." *Front. Built Environ.* 3 (Jun): 32. https://doi.org/10.3389/fbuil.2017.00032.
Priest, G., et al. 2013. *Tsunami inundation scenarios for Oregon*. Portland, OR: Oregon Dept. of Geology and Mineral Industries.
Sanderson, D., S. Kameshwar, N. Rosenheim, and D. Cox. 2021. "Deaggregation of multi-hazard damages, losses, risks, and connectivity: An application to the joint seismic-tsunami hazard at Seaside, Oregon." *Nat. Hazard.* 109 (2): 1821–1847. https://doi.org/10.1007/s11069-021-04900-9.
Shiraki, N., M. Shinozuka, J. Moore, S. Chang, H. Kameda, and S. Tanaka. 2007. "System risk curves: Probabilistic performance scenarios for highway networks subject to earthquake damage." *J. Infrastruct. Syst.* 13 (1): 43–54. https://doi.org/10.1061/(ASCE)1076-0342(2007)13:1(43).
SPUR (San Francisco Planning & Urban Research Association). 2009. *The resilient city: Defining what San Francisco needs from its seismic mitigation policies*. San Francisco: SPUR.
Sun, W., P. Bocchini, and B. D. Davison. 2018. "Resilience metrics and measurement methods for transportation infrastructure: The state of the art." *Sustainable Resilient Infrastruct.* 5 (3): 168–169. https://doi.org/10.1080/23789689.2018.1448663.
Thacker, S., R. Pant, and J. Hall. 2017. "System-of-systems formulation and disruption analysis for multi-scale critical national infrastructures." *Reliab. Eng. Syst. Saf.* 167 (Nov): 30–41. https://doi.org/10.1016/j.ress.2017.04.023.
US Census Bureau. 2019. "Table DP05: ACS demographic and housing estimates." Accessed February 22, 2021. https://data.census.gov/cedsci/.
Wang, W., and J. van de Lindt. 2021. "Quantitative modeling of residential building disaster recovery and effects of pre- and post-event policies." *Int. J. Disaster Risk Reduct.* 59 (Jun): 102259. https://doi.org/10.1016/j.ijdrr.2021.102259.
Wu, J., H. Deng, Y. Tan, and D. Zhu. 2007. "Vulnerability of complex networks under intentional attack with incomplete information." *J. Phys. A: Math. Theor.* 40 (11): 2665–2671. https://doi.org/10.1088/1751-8113/40/11/005.
Yang, T., J. Moehle, B. Stojadinovic, and A. Der Kiureghian. 2009. "Seismic performance evaluation of facilities: Methodology and implementation." *J. Struct. Eng.* 135 (10): 1146–1154. https://doi.org/10.1061/(ASCE)0733-9445(2009)135:10(1146).
Zhang, N., and A. Alipour. 2020. "Multi-scale robustness model for highway networks under flood events." *Transp. Res. Part D Transp. Environ.* 83 (Jun): 102281. https://doi.org/10.1016/j.trd.2020.102281.
Zhang, Q., M. Northridge, Z. Jin, and S. Metcalf. 2018. "Modeling accessibility of screening and treatment facilities for older adults using transportation networks." *Appl. Geogr.* 93 (Apr): 64–75. https://doi.org/10.1016/j.apgeog.2018.02.013.
Zhang, X., E. Miller-Hooks, and K. Denny. 2015. "Assessing the role of network topology in the transportation network resilience." *J. Transp. Geogr.* 46 (Jun): 35–45. https://doi.org/10.1016/j.jtrangeo.2015.05.006.
Zou, Q., and S. Chen. 2020. "Resilience modeling of interdependent traffic-electric power system subject to hurricanes." *J. Infrastruct. Syst.* 26 (1): 04019034. https://doi.org/10.1061/(ASCE)IS.1943-555X.0000524.